Chapter 4

Numerical results

This chapter is concerned with the numerical implementation of the control concept presented in the previous chapter, i.e. state space adaptive control. The simulation of the entire control concept is carried out using a nonlinear model as described in detail in Chapter 2 with the simulation parameters given in Appendix D.2. The nonlinear model and the control algorithms are implemented by the numerical simulation tool MATLAB/SIMULINK [MATLAB, 1992, SIMULINK, 1992].

The estimation algorithm, however, was derived for a linear state space model based on a linear actuator model. Therefore, this simplification has to be justified by means of simulation, before the state space adaptive control concept is implemented.

4.1 Current control loop

In order to derive the linear state space model for the rotor bearing system used for the controller design in Chapter 3 the current control loop was introduced in Section 2.3.2. This is a necessary condition in order to treat the magnetic actuator as a gain with respect to the control current and as a spring with a negative coefficient with respect to the rotor displacement. However, this simplification is only justified, if the bandwidth of the current control loop covers the frequency band of the position control loop. Therefore, the bandwidth of the current control loop has to be tested.

In Chapter 2 the entire nonlinear model of a rigid rotor suspended in active magnetic bearings was depicted by Fig. 2.2. For the simulation of the current control loop, only the electric signal path is under investigation as depicted in Fig. 4.1. The nonlinear model was implemented as a MATLAB/SIMULINK model with its block diagrams shown in Appendix D.1. The parameters used for simulation are given in Tab. 2.1 for the digital to analogue converter, in Tab. 2.2 for the pulse width modulator, in Tab. 2.3 for the actuator, and in Tab. 2.7 for the analogue to digital converter.

For the sake of the controller design, a linear model of the current control loop was derived in Section 2.3.2. In the following, the numerical results for the controller design of only one channel are presented.

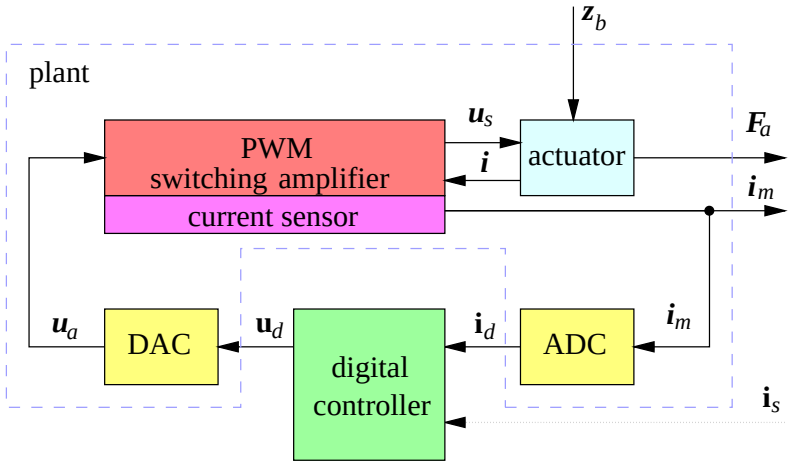

inputs: i_s desired current
z_b rotor position

output: F_a actuator forces
i_m measured current

internal variables:

u_d digital control voltage
u_a analogue control voltage
u_s switched voltage
i current
i_m measured current
i_d sampled current

Figure 4.1: Block diagram of the current control loop with the inputs "rotor position" and "current set point", the output "actuator force" and "measured current", and all internal variables and subsystems. This loop controls 8 current channels.

4.1.1 Current controller design

In Section 2.3.2 the open loop transfer function was derived for the current control loop as

$$G_o(s) = \frac{K_c\, K_a\, \mathcal{R}_0}{N^2\, s\, (1 + \frac{T_s}{2}\, s)},$$

and with all known parameters inserted

$$G_o(s) = K_c\, \frac{2.17005 \cdot 10^3}{s\, (1 + 0.00005\, s)}.$$

The controller gain K_c is determined using the frequency plot as shown in Fig. 4.2 with a phase margin of 70 deg which corresponds to an aperiodic transition after a set point change. The high value for the phase margin is chosen, because in an experimental implementation additional time delay or saturation decreases the phase margin anyway. For a large phase margin stability can be guaranteed for a wide range of operation.

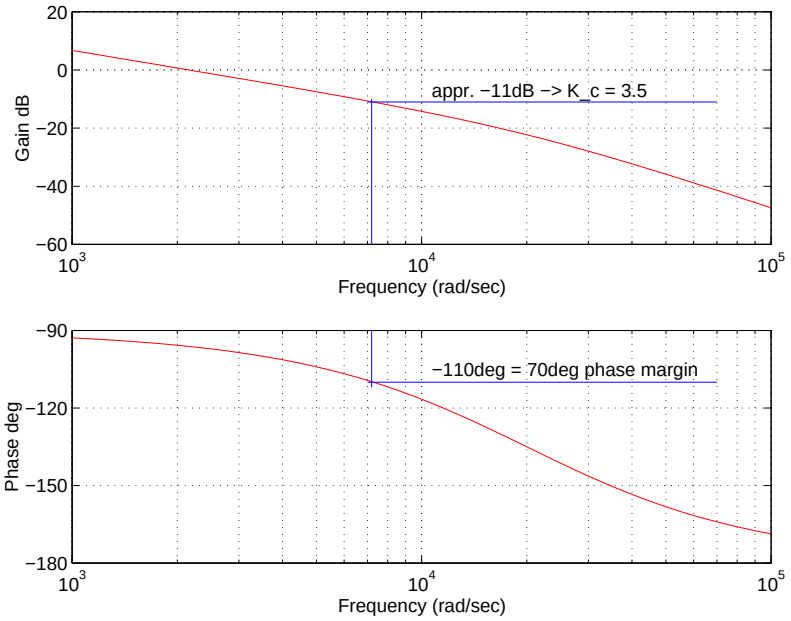

Figure 4.2: Bode plot of the open current loop transfer function with the controller gain $K_c = 3.5$.

The controller gain has been found to be $K_c = 3.5$ for a phase margin of 70 deg. For this second order system the closed loop transfer function can be calculated as

$$G_{ii_s}(s) = \frac{i_m}{i_s} = \frac{1.519 \cdot 10^8}{s^2 + 2 \cdot 10^4\, s + 1.519 \cdot 10^8},$$

with the undamped closed loop eigenfrequency $\omega_n = 12,325\,1/\mathrm{s}$ and a damping factor of $\zeta = 0.81$. For this frequency and the corresponding damping factor the time delay for a unit step response can be calculated as $320\,\mu\mathrm{s}$ for a linear system. Using a bode plot for the closed loop system, the $-3\,\mathrm{dB}$ limit can be found for a frequency of $10,367\,1/\mathrm{s}$ or a bandwidth of approximately $1,650\,\mathrm{Hz}$.

The current controller, designed in the analogue time domain, has to be transformed into the discrete time domain for an implementation as a digital controller. Using the Tustin transformation

$$s = \frac{2}{T_s}\,\frac{1 - z^{-1}}{1 + z^{-1}},$$

the digital controller operating at the sampling time T_s can be presented as

$$G_{c_d}(z) = \frac{b_0 + b_1\, z^{-1}}{1 - z^{-1}}.$$

with the coefficients

$$\begin{aligned} b_0 &= \frac{K_c\, T_s\, r\, \mathcal{R}_0}{N^2\, 2} + K_c, \\ b_1 &= \frac{K_c\, T_s\, r\, \mathcal{R}_0}{N^2\, 2} - K_c. \end{aligned}$$

4.1.2 Current controller implementation

As already mentioned, the controller is implemented digitally in the DSP for 8 channels, i.e. for 2 bearing actuators in this investigation. Inputs to the control loops are the sampled coil currents $\mathbf{i}_d$, outputs of all control loops are the control variables $\mathbf{u}_d$. The controller for one channel is implemented in a recursive form such that

$$u_c(k) = u_c(k-1) + b_0\, e(k) + b_1\, e(k-1)$$

with the set point error at time k as $e(k) = i_s(k) - i_d(k)$ with $i_d(k)$ being the measured and sampled coil current. The controller output u_c is shifted by 2.5 V to meet the range of the DACs of 0-5 V with $u_d = u_c + 2.5\,\mathrm{V}$. The parameters of the resulting current controller are presented in Tab. 4.1.

Table 4.1: Parameters of current controller.

T_s	sampling time	100	μs
K_c	Controller gain	3.5	-
b_0	controller coefficient for z^0	3.5101	-
b_1	controller coefficient for z^{-1}	-3.4899	-

4.1.3 Initial values for simulation

For a simulation run, all initial states have to be chosen in advance. The simulation is started form a precalculated point of operation determined by $i_0 = 4\,\mathrm{A}$, and the rotor position set equal to zero ($\mathbf{z}_b = \mathbf{0}\,\mathrm{m}$), i.e. an air gap length for each electromagnet of $l_0 = 500\,\mu\mathrm{m}$. All further initial variables can be calculated upon these values following the equations in Section 2.3.

The current control loop starts with all internal and state variables like the initial flux Φ_0 and the control voltage u_c initialised properly. The initial control variable u_c can be computed as $u_{c_0} = r\, i_0\,\mathrm{V}$, the initial flux as $\Phi_0 = 0.4254 \cdot 10^{-3}\,\mathrm{Vs}$.

A fact which has to be mentioned is that the voltage output is $u_d = 2.5\,\mathrm{V}$ for a control voltage of $u_c = 0\,\mathrm{V}$, because the range of the DAC is 0-5 V. Additionally, for the point of operation defined by $i_0 = 4\,\mathrm{A}$, the mean voltage for the coil is $u_0 = r \cdot i_0 = 3.2\,\mathrm{V}$, or prior to the amplifier, $u_{c_0} = \frac{u_0}{K_a} = 0.1067\,\mathrm{V}$. This means that the digital control voltage for the point of operation is $u_{d_0} = u_{c_0} + 2.5 = 2.607\,\mathrm{V}$.

4.1.4 Simulation results

In order to determine the bandwidth of the current control loop, simulation runs have been carried out. This is possible by both a step response and frequency analysis.

Current step response

Using all previous parameters, a current step response was simulated for one channel only. From the point of operation of 4 A current step responses to 4.25 A, 4.5 A and 5 A were simulated. The corresponding current plots can be seen in Fig. 4.3 and the plots of the control voltage in Fig. 4.4.

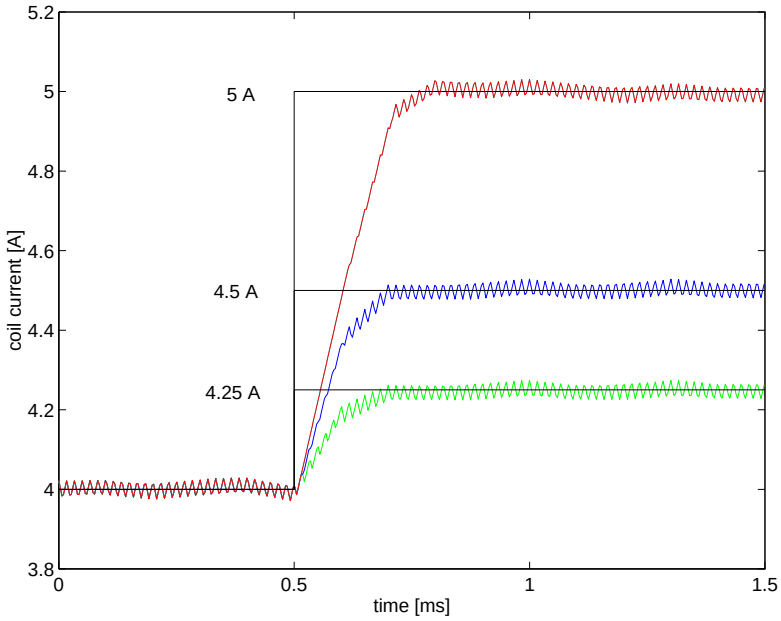

Figure 4.3: Step response of the controlled current after a set point change from 4 A *to* 4.25 A, 4.5 A, *and* 5 A.

As it can be seen in Fig. 4.3, it takes approximately three sample intervals, i.e. about 300 μs until the set point is reached, which corresponds well to the predicted value. If the step is smaller than approximately $\frac{2.5}{K_c} = 0.71$ A, then the system undergoes no saturation and the control loop is linear. If the set point change is higher than 0.71 A, the control voltage runs into saturation and the time consumed to reach the set point is determined by the slope

$$\frac{di}{dt}\Big|_{\max} = \frac{\text{switching voltage } U_s}{\text{initial inductivity } L_0} = 5.4 \cdot 10^3 \text{ A/s}$$

such that

$$\Delta T = \left(\frac{di}{dt}\Big|_{\max}\right)^{-1} \Delta i \approx 185 \cdot 10^{-6} \cdot \Delta i \text{ s}$$

This means that for a step of 1 A, it takes about 185 μs until the set point is reached which corresponds well to the simulation result in Fig. 4.3. The saturation of the control voltage can be seen in Fig. 4.4.

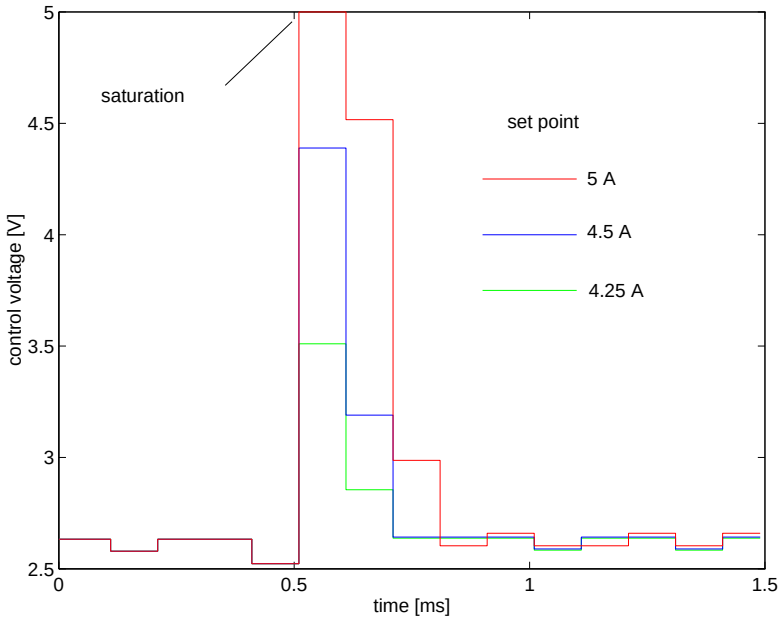

Figure 4.4: Step response of the control voltage after a set point change from 4 A *to* 4.25 A, 4.5 A, *and* 5 A.

Since a PI-controller is implemented in a digital version, no set point error remains, but the control current is corrupted by a large ripple due to the switching amplifier operating at a frequency of 60 kHz. The ripple could only be reduced if the switching frequency is increased, or if the switching voltage is decreased. In the latter case, the dynamics suffers from a small current slope.

In addition, the current signals contaminated by the large ripple contain frequencies beyond the Nyquist frequency. This effect is probably due to the presence of nonlinear elements as the quantisers (ADC, and DAC) and to an aliasing effect. Therefore, a low pass filter should be used to cancel the switching frequency and all harmonics. It is advisable to implement this filter as an analogue filter. Unfortunately this filter causes an additional phase lag which is the reason why it was not implemented in this simulation. A better solution is to sample the current at a higher frequency and apply down sampling techniques on the resulting digital signal. This yields a signal at the original sampling frequency of higher quality.

Frequency response

Here, the set point for the current control loop is a sinusoidal signal of 0.25 A, 0.5 A and 1 A amplitude with variable frequency at the point of operation of 4 A. In Fig. 4.5 the frequency plot can be seen. The frequency range of this plot is limited by the Nyquist frequency, i.e. half the sampling frequency of 10 kHz. The bandwidth of the current control loop depends on the amplitude as can be expected for a nonlinear behaviour due to the saturation of the control voltage. For an amplitude range up to 0.71 A, the

−3 dB limit is about at 1.7 kHz, which corresponds well to the predicted bandwidth determined by Eqn.(2.52).

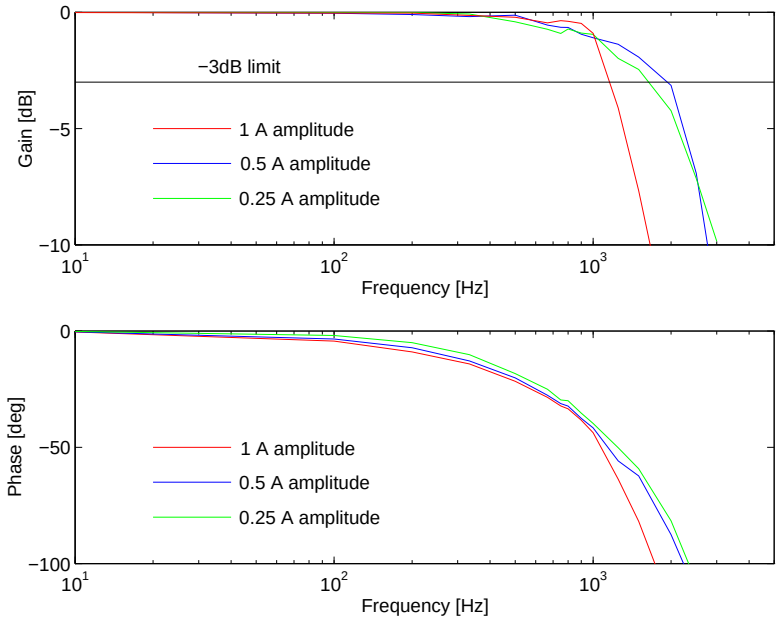

Figure 4.5: Frequency response of the closed current control loop excited by a sinusoidal signal of amplitude 0.25 A, 0.5 A, *and* 1 A.

For larger current amplitudes $\bar{A}$ the limit frequency depends on the maximal current slope available such that

$$\omega_s \, \bar{A} = \left. \frac{di}{dt} \right|_{\max}.$$

The maximum frequency the controlled variable can follow is

$$f_s = \frac{\omega_s}{2\pi} \approx \frac{1}{\bar{A}} \, 865 \, \text{Hz}.$$

Up to now only the amplitude was investigated to determine the bandwidth of the current control loop. However, as can be seen in Fig. 4.5, the phase lag is approximately 90 deg for a frequency of 1.7 kHz. Considering the phase lag, the real bandwidth is limited to 250 Hz with a maximum phase lag of 10 deg. Below this frequency the response transfer function can be treated as a gain with respect to the control current.

4.2 The linear actuator model

Once the current controller loop has been tested, the actuator forces and the typical coefficients for an active magnetic bearing can be computed using simulation as well. Using the derivation in Section 2.3.4, these coefficients for an active magnetic bearing with linearised characteristics can be calculated by

$$\begin{aligned} K_i &= \frac{4\,N^2\,i_0}{\mathcal{R}_0^2\,\mu_0\,A_l}\cos\frac{\alpha}{2}, \\ K_s &= -\frac{8\,N^2\,i_0^2}{\mathcal{R}_0^3\,\mu_0^2\,A_l^2}\cos\frac{\alpha}{2}. \end{aligned}$$

Inserting the initial values for the given actuator of Tab. 2.3 yields the coefficients for the active magnetic bearing as given in Tab. 4.2.

Table 4.2: Parameters of the linearised active magnetic bearing.

K_i	current gain	190.04	N/A
K_s	position stiffness	$-1.4138\,10^6$	N/m

The predicted values for the coefficients can then be compared with the values determined by means of simulation.

4.2.1 Current gain of the magnetic actuator forces

The rotor is held in a fixed position $\mathbf{z}_b = \mathbf{0}\,\mathrm{m}$ at the point of operation defined by the bias current. If the control current $\mathbf{i}_c$ is varied in one direction, the actuator acts as a gain with a certain coefficient, generally referred to as force current gain. The actuator forces $\mathbf{F}_a = [F_x, F_y]$ can be obtained by

$$\mathbf{F}_a = \boldsymbol{K}_i\,\mathbf{i}_c$$

with the control currents $\mathbf{i}_c = [i_x, i_y]$ in x and y direction. $\boldsymbol{K}_i$ is diagonal matrix of proper dimension with the diagonal entries K_i, the current gain factor.

An underlying current control loop is required for all coils of the actuator. The reference signals of each current control loop is computed according to Eqn.(2.67) to Eqn.(2.70) given in Section 2.3.4 from the control current $\mathbf{i}_c$.

Current step response of the magnetic actuator force

A step response simulation for one actuator was carried out for a control current i_x of 0.25 A, 0.5 A, and 1 A in x-direction. For reasons of symmetry, the response in y-direction is similar and therefore not simulated. The corresponding plot can be

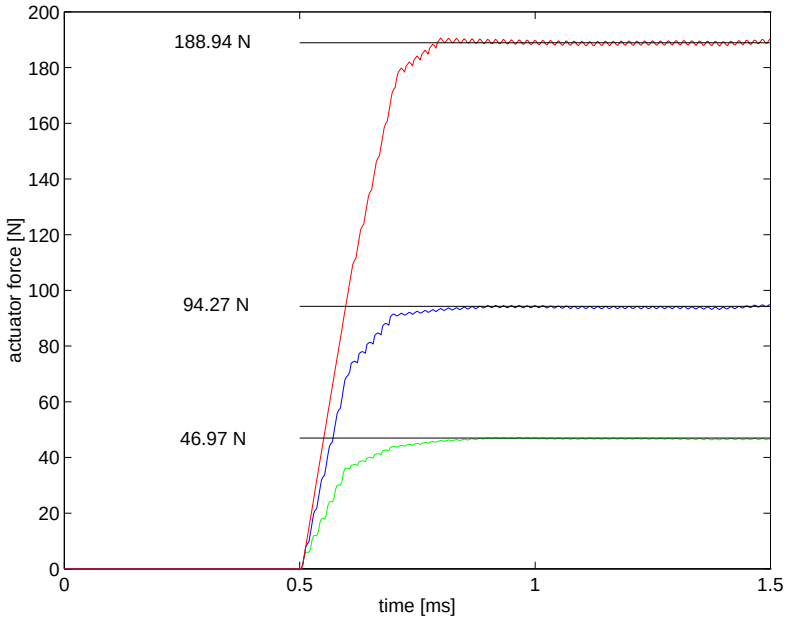

Figure 4.6: Step response of the actuator force for a control current steps of 0.25 A, 0.5 A, *and* 1 A *at* $t = 0.5$ ms.

seen in Fig. 4.6. In comparison with the precalculated values, the current gain is $K_i = 188.94\,\mathrm{N/A}$ for a step from $i_x = 0\,\mathrm{A}$ to $i_x = 1\,\mathrm{A}$, which is about 0.6 % below the precalculated value. For smaller steps, e.g. of $i_x = 0.25\,\mathrm{A}$, the resulting gain is approximately $K_i = 187.90\,\mathrm{N/A}$, for a step of $i_x = 0.5\,\mathrm{A}$, the resulting gain is approximately $K_i = 188.54\,\mathrm{N/A}$. Thus, the current factor is almost invariant of the magnitude of the step applied. In addition, the value determined by means of simulation is slightly smaller than the precalculated one. This is probably due to the fact that within the simulation the relative permeability of all magnetic materials depends on the flux itself. Therefore, the real flux is a little smaller than the computed flux for $\mu = \mu_0\,\mu_r = \text{constant}$.

Current frequency response of the magnetic actuator force

If the actuator is excited by a sinusoidal control current, the actuator forces is sinusoidal as well with a certain gain and a certain phase lag. A plot with the sinusoidal control current and the resulting actuator force can be seen in Fig. 4.7. The current gain K_i can be obtained by the slope of the main axis of the ellipsis for the excitation frequency $\to 0$. It can be seen that this gain decreases with increasing amplitude of the control current. This is due to the limited bandwidth of the current control loop. More obviously, the increasing phase lag can be seen in the phase plot in Fig. 4.7. The consequence is that the actuator can only be treated as a gain up to a frequency of about 250 Hz.

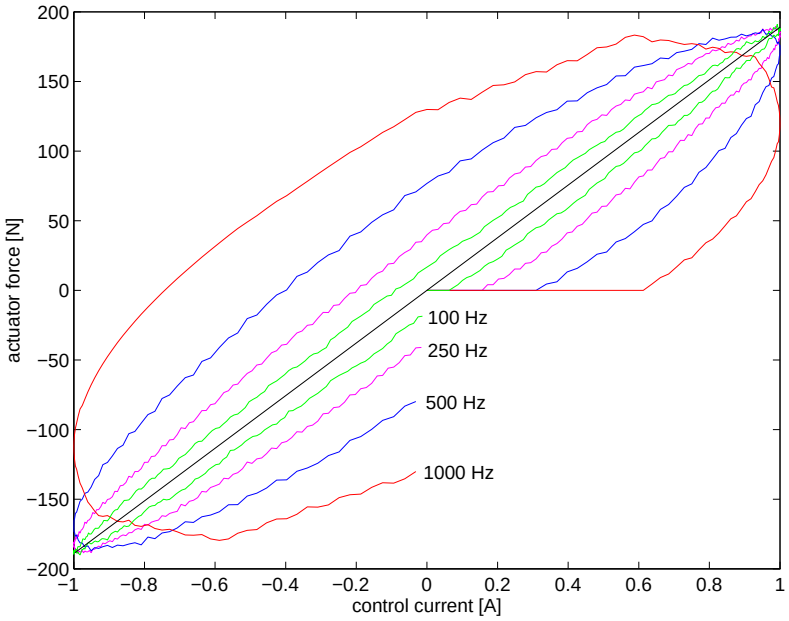

Figure 4.7: Plot of the sinusoidal excitation of control current at a amplitude of 1 A *versus the resulting actuator forces at* 100 Hz, 250 Hz, 500 Hz, *and* 1000 Hz.

4.2.2 Position Stiffness of the magnetic actuator forces

The rotor displacement and thus the change of the air gaps within the several electromagnets can be viewed as disturbance for the current control loop (see Fig. 2.8 and Fig. 2.9). This loop controls the current in all electromagnets at the point of operation for varying rotor positions. If the position of the rotor changes, the actuator reacts as a negative spring with a specific coefficient at the point of operation. The actuator forces $\mathbf{F}_a = [F_x, F_y]$ can be obtained by

$$\mathbf{F}_a = \boldsymbol{K}_s \, \mathbf{z}_b$$

with the rotor position $\mathbf{z}_b = [x, y]$ and the diagonal matrix $\boldsymbol{K}_s$ with K_s the position stiffness as diagonal entry. This position coefficient for an actuator can be calculated by a steady state simulation as well as by frequency analysis.

Displacement step response of the magnetic actuator force

A step response for one actuator was carried out for a rotor displacement in one direction x of 25 μm, 50 μm and 100 μm. The corresponding plots can be seen in Fig. 4.8. The mean values for all step responses can be used to compute the position stiffness which in this case, depends on the magnitude of the step. For a step of 10 μm, the resulting stiffness is $1.40 \cdot 10^6$ N/m which is quite close to the predicted value of $1.4138\,10^6$ N/m. For a step of 50 μm the position stiffness is $1.4258\,10^6$ N/m, and for

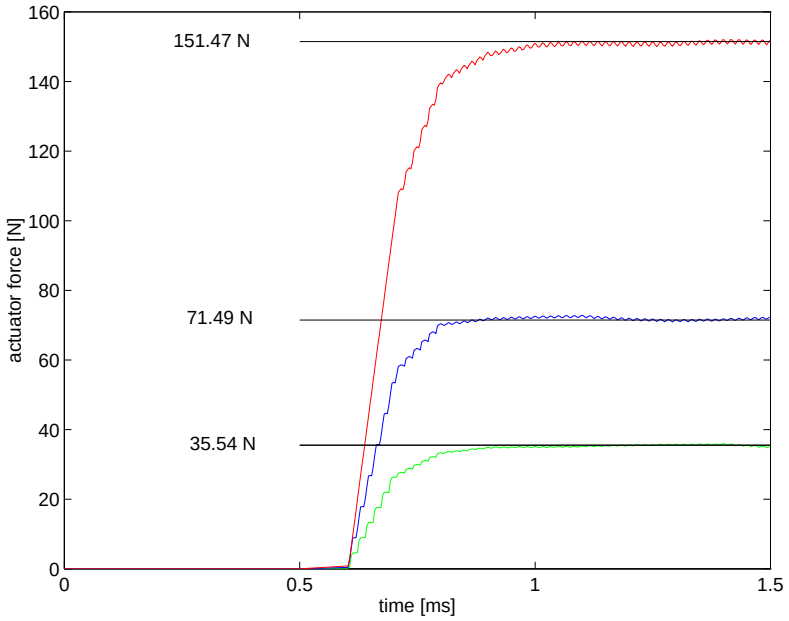

Figure 4.8: Step response of the controlled actuator for rotor displacements of $10\,\mu$m, $50\,\mu$m, *and* $100\,\mu$m *at* $t = 0.5$ ms.

a step of $100\,\mu$m it is $1.5090\,10^6$ N/m. This means that the stiffness increases with increasing rotor displacement. Therefore, simulations have been carried out for various steps of different magnitudes. The corresponding plot can be seen in Fig. 4.9. The pro-

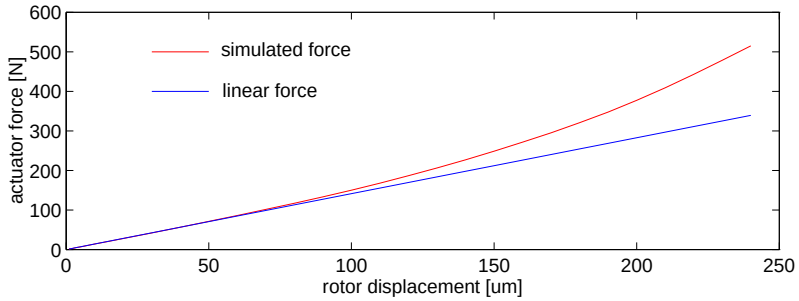

Figure 4.9: Actuator force as function of the rotor displacement for a given point of operation defined by $i_0 = 4$ A.

gressive behaviour can be explained by the dependence of the position stiffness on the air gap length which directly influences the magnetic flux. If the current is controlled to be constant, the flux increases whenever the reluctance decreases.

In Fig. 4.8 it can be observed that it takes approximately one sampling interval until the actuator force increases. As mentioned before, the varying rotor displacement and thus the varying air gap within the magnetic path can be viewed as disturbance for

the current control loop. The entire energy of the magnetic path is stored in the flux. If the rotor is moved in a stepwise manner, the flux does not change abruptly, i.e. the actuator force does not change abruptly either. Since an ideal voltage source is assumed, the step of the rotor displacement does not introduce a voltage, but changes the rate of the flux and the current instantaneously to keep the energy constant. After the current control loop has managed to keep the current at the point of operation, the entire energy has changed according to the definition of the flux depending on the current and the air gap. Thus, the resulting force increases as fast as the current loop can control the coil current.

Frequency response of the magnetic actuator force in terms of the rotor displacement

If the actuator is excited by a sinusoidal signal of the rotor displacement, the actuator forces is sinusoidal as well with a certain gain and a certain phase lag. A phase plane plot can be seen in Fig. 4.10. The resulting stiffness decreases with increasing

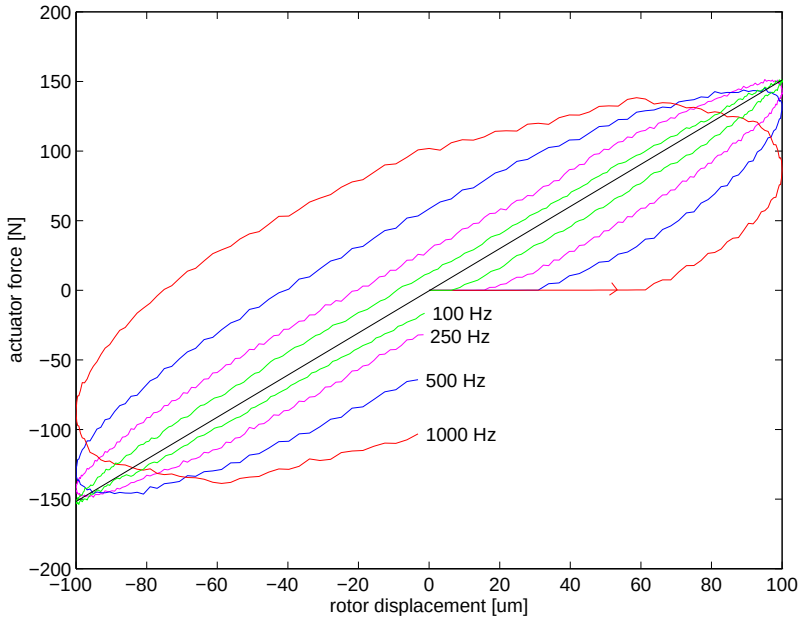

Figure 4.10: Plot of the sinusoidal excitation of the rotor displacement at a amplitude of 100 µm *versus the resulting actuator forces at* 100 Hz, 250 Hz, 500 Hz *and* 1000 Hz.

frequency starting at approximately $1.52 \cdot 10^6$ N/m. Additionally, the phase lag increases according to the current control loop which generates the elliptic shape of the force to displacement curve.

In this section it has been shown that the actuator controlled by a current control loop can be treated as a gain up to a frequency of approximately 250 Hz. Thus, the

derivation of a linear state space model is justified. This model can then be used for a state space controller, as long as the frequency band of the resulting closed loop of the position controller is below the frequency band of the the current control loop.

4.3 The linear state space model

After the linearity of the actuator has been shown in the previous section by means of simulation, the deterministic linear state space plant model can be established. This model is used for the state space adaptive control concept. Note that for this state space model an internal current control loop is always required.

To keep the rotor in a centred position, the steady state load has to be compensated by an additional control current such that

$$\mathbf{i}_{c_w} = \boldsymbol{K}_i^{-1} \cdot \mathbf{F}_w,$$

with the rotor weight components in bearing coordinates

$$\mathbf{F}_w = [0,\, -141.8302,\, 0,\, -140.3839,\,]^T \text{ N}.$$

This is necessary to provide the disturbances of zero mean which is an assumption for both the adaptive control concept and the predictor. Heuristically speaking, the predictor cannot render the reaction of the system to be observed, if there is no model available describing how the disturbances act on the system. The resulting steady state control current

$$\mathbf{i}_{c_w} = [0,\, -0.7463,\, 0,\, -0.7387]^T \text{ A}$$

is simply added to the dynamic control current in order to compensate the steady state load. Note that the point of operation is shifted regarding the steady state coil currents which affects the current gain and the position stiffness.

4.3.1 System matrices

The continuous time state space model was derived in Chapter 2 in the form

$$\begin{aligned} \dot{\boldsymbol{x}} &= \boldsymbol{A} \cdot \boldsymbol{x} + \boldsymbol{B} \cdot \boldsymbol{u}, \\ \boldsymbol{y} &= \boldsymbol{C} \cdot \boldsymbol{x} + \boldsymbol{v}, \end{aligned}$$

with the state vector $\boldsymbol{x} = [\boldsymbol{z}_b, \dot{\boldsymbol{z}}_b]^T$ and the output vector $\boldsymbol{y} = k_m\,(\boldsymbol{z}_b + \boldsymbol{v})$. A virtual sensor gain k_m converts the system states from m into μm for numerical reasons. The concentrated measurement noise is assumed to have a maximum deflection of 1 μm. Inserting all rotor parameters, an initial non-conservative cross-coupling stiffness parameter $k_n = 0\,\text{N/m}$ and the coefficients for the active magnetic bearing, the system

matrices are (in the following numbers consistently SI-units are applied)

$$\boldsymbol{A} = \begin{bmatrix} 0 & 0 & 0 & 0 & 1 & 0 & 0 & 0 \\ 0 & 0 & 0 & 0 & 0 & 1 & 0 & 0 \\ 0 & 0 & 0 & 0 & 0 & 0 & 1 & 0 \\ 0 & 0 & 0 & 0 & 0 & 0 & 0 & 1 \\ 1.4252e3 & 0.0 & -0.4519e3 & 0.0 & 0 & 0 & 0 & 0 \\ 0.0 & 1.4252e3 & 0.0 & -0.4519e3 & 0 & 0 & 0 & 0 \\ -0.4519e3 & 0.0 & 1.4446e3 & 0.0 & 0 & 0 & 0 & 0 \\ 0.0 & -0.4519e3 & 0.0 & 1.4446e3 & 0 & 0 & 0 & 0 \end{bmatrix},$$

$$\boldsymbol{B} = \begin{bmatrix} 0 & 0 & 0 & 0 \\ 0 & 0 & 0 & 0 \\ 0 & 0 & 0 & 0 \\ 0 & 0 & 0 & 0 \\ 19.1573 & 0.0 & -6.0748 & 0.0 \\ 0.0 & 19.1573 & 0.0 & -6.0748 \\ -6.0748 & 0.0 & 19.4173 & 0.0 \\ 0.0 & -6.0748 & 0.0 & 19.4173 \end{bmatrix},$$

$$\boldsymbol{C} = \begin{bmatrix} 1e6 & 0 & 0 & 0 & 0 & 0 & 0 & 0 \\ 0 & 1e6 & 0 & 0 & 0 & 0 & 0 & 0 \\ 0 & 0 & 1e6 & 0 & 0 & 0 & 0 & 0 \\ 0 & 0 & 0 & 1e6 & 0 & 0 & 0 & 0 \end{bmatrix}.$$

Using a sampling time of $T_s = 100\,\mu$s and the transformation $\mathbf{T}$ as derived in Appendix A, the discrete time state space model in controller canonical form results in

$$\begin{aligned} \mathbf{x}(k+1) &= \mathbf{A}\,\mathbf{x}(k) + \mathbf{B}\,\mathbf{u}(k), \\ \mathbf{y}(k) &= \mathbf{C}\,\mathbf{x}(k), \end{aligned}$$

with the state vector is $\mathbf{x}(k)$. The input vector $\mathbf{u}(k)$ is the sampled input vector $\boldsymbol{u}(t)$ and the output vector $\mathbf{y}(k)$ is the sampled vector $\boldsymbol{y}(t)$. The system matrices are given by

$$\mathbf{A} = \begin{bmatrix} 0 & 1 & 0 & 0 & 0 & 0 & 0 & 0 \\ -1.0 & 2.0014 & 0.0 & 0.0 & 0.0 & -0.0005 & 0.0 & 0.0 \\ 0 & 0 & 0 & 1 & 0 & 0 & 0 & 0 \\ 0.0 & 0.0 & -1.0 & 2.0014 & 0.0 & 0.0 & 0.0 & -0.0005 \\ 0 & 0 & 0 & 0 & 0 & 1 & 0 & 0 \\ 0.0 & -0.0005 & 0.0 & 0.0 & -1.0 & 2.0014 & 0.0 & 0.0 \\ 0 & 0 & 0 & 0 & 0 & 0 & 0 & 1 \\ 0.0 & 0.0 & 0.0 & -0.0005 & 0.0 & 0.0 & -1.0 & 2.0014 \end{bmatrix},$$

$$\mathbf{B} = \begin{bmatrix} 0 & 0 & 0 & 0 \\ 1 & 0 & 0 & 0 \\ 0 & 0 & 0 & 0 \\ 0 & 1 & 0 & 0 \\ 0 & 0 & 0 & 0 \\ 0 & 0 & 1 & 0 \\ 0 & 0 & 0 & 0 \\ 0 & 0 & 0 & 1 \end{bmatrix},$$

$$\mathbf{C} = \begin{bmatrix} 0.096 & 0.096 & 0.0 & 0.0 & -0.030 & -0.030 & 0.0 & 0.0 \\ 0.0 & 0.0 & 0.096 & 0.096 & 0.0 & 0.0 & -0.030 & -0.030 \\ -0.030 & -0.030 & 0.0 & 0.0 & 0.097 & 0.097 & 0.0 & 0.0 \\ 0.0 & 0.0 & -0.030 & -0.030 & 0.0 & 0.0 & 0.097 & 0.097 \end{bmatrix}.$$

Note that some entries of the state space matrices are not necessarily equal to zero for numerical reasons which is indicated by the number 0.0 instead of simply 0. The latter is used, if the controller canonical form requires a zero entry.

4.3.2 State space controller

Since the system is open-loop unstable, a controller has to be designed in advance. This has been done according to the nominal system without destabilising cross-coupling effects of the rotor. The poles of the closed loop system have been placed at $z_i = 0.97$, or in the continuous complex plane to $s_i = -288\,1/\mathrm{s}$, which would meet the eigenvalue for a mass-spring-system with a negative stiffness factor of the magnetic bearing.

Inputs to the controller are the estimated system states $\hat{\mathbf{x}}(k)$ provided by the predictor, and the rotor positions $\mathbf{y}(k)$ determined by equation Eqn.(2.80) and Eqn.(2.79). Output of the position controller is the control current $\mathbf{u} = \mathbf{i}_c$ which is used to compute the reference signals of each current control loop according to Eqn.(2.67) to Eqn.(2.70) as presented in Section 2.3.4 for one actuator.

P-structure

The characteristic polynomial for the closed loop system can be easily calculated with all system poles at $z_i = 0.97$ as

$$P^{(ii)}(z) = z^2 - 1.9382\,z + 0.9392.$$

The control matrix $\mathbf{K}_x$ for the control law

$$\mathbf{u}(k) = -\mathbf{K}_x\,\mathbf{x}(k) + \mathbf{K}_w\,\mathbf{w}(k)$$

can then be computed using Eqn.(3.70) to Eqn.(3.71) as

$$\mathbf{K}_x = \begin{bmatrix} -0.061 & 0.063 & 0.0 & 0.0 & 0.0 & -0.001 & 0.0 & 0.0 \\ 0.0 & 0.0 & -0.061 & 0.063 & 0.0 & 0.0 & 0.0 & -0.001 \\ 0.0 & -0.001 & 0.0 & 0.0 & -0.061 & 0.063 & 0.0 & 0.0 \\ 0.0 & 0.0 & 0.0 & -0.001 & 0.0 & 0.0 & -0.061 & 0.063 \end{bmatrix}.$$

Using Eqn.(3.76) the feed forward gain can be computed as

$$\mathbf{K}_w = \begin{bmatrix} 0.0055 & 0.0 & 0.0017 & 0.0 \\ 0.0 & 0.0055 & 0.0 & 0.0017 \\ 0.0017 & 0.0 & 0.0055 & 0.0 \\ 0.0 & 0.0017 & 0.0 & 0.0055 \end{bmatrix}.$$

Since the controller design is carried out for the nominal system without cross-coupling effects, the stability region for this controller design can be shown by a root locus plot with the non-conservative stiffness coefficient k_n as parameter. The resulting plot can be seen in Fig. 4.11 with k_n starting at zero for the nominal system and increasing up to $10^7\,\mathrm{N/m}$. If $k_n = 0\,\mathrm{N/m}$, all 8 poles are identically located at $z_i = 0.97$. If k_n is larger than $4.2 \cdot 10^6\,\mathrm{N/m}$, the system becomes unstable unless the controller is adapted to the new parameters.

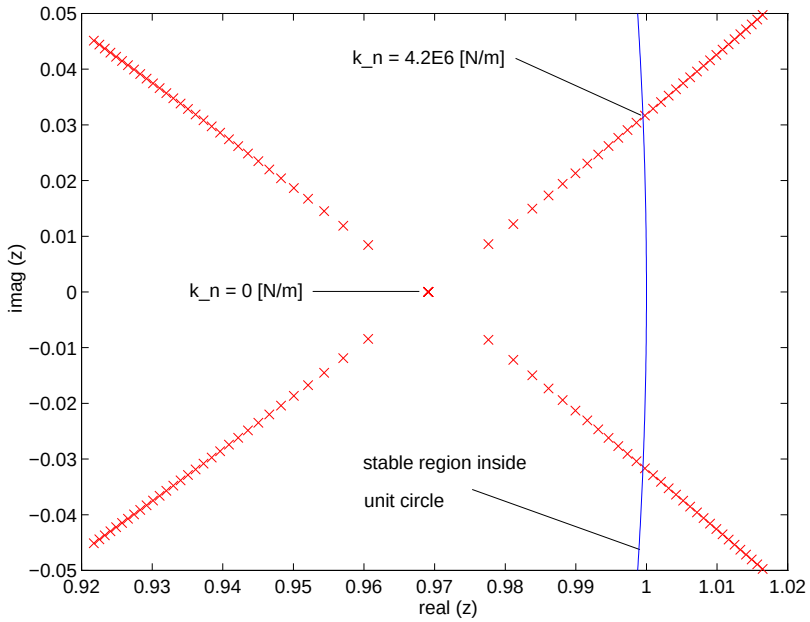

Figure 4.11: Root locus of the closed loop system with varying non-conservative stiffness parameter k_n from $0\,\mathrm{N/m}$ to $10^7\,\mathrm{N/m}$, and with constant controller parameters. The closed loop system starting at $z_i = 0.97$ is unstable for $k_n > 4.2 \cdot 10^6\,\mathrm{N/m}$.

PI-structure

The characteristic polynomial of the closed loop system with additional integrative feedback can be easily calculated with all system poles at $z_i = 0.97$ as

$$P_I^{(ii)}(z) = z^3 - 2.9073\,z^2 + 2.8175\,z - 0.9101.$$

The control law for the PI-structure is given by

$$\begin{aligned} \mathbf{u}(k) &= \mathbf{u}_I(k) - \mathbf{K}_x\,\mathbf{x}(k), \\ \mathbf{u}_I(k+1) &= \mathbf{u}_I(k) + \mathbf{K}_I\,\mathbf{e}(k), \\ \mathbf{e}(k) &= \mathbf{w}(k) - \mathbf{y}(k). \end{aligned}$$

Using Eqn.(3.93) the controller matrix $\mathbf{K}_I$ for the initial system is

$$\mathbf{K}_I = 10^{-3} \begin{bmatrix} 0.1709 & 0.0 & 0.0535 & 0.0 \\ 0.0 & 0.1709 & 0.0 & 0.0535 \\ 0.0535 & 0.0 & 0.1687 & 0.0 \\ 0.0 & 0.0535 & 0.0 & 0.1687 \end{bmatrix}.$$

The coefficients of the polynomial for the closed loop system without integrative feedback have been determined using Eqn.(3.94) and Eqn.(3.95). For the nominal system which consists of four identical subsystems, these coefficients determine the new polynomial for the system without integrative feedback

$$P^{(ii)}(z) = z^2 - 1.9073\,z + 0.9101.$$

With these coefficients the controller matrix $\mathbf{K}_x$ can be obtained from Eqn.(3.70) and Eqn.(3.71) as

$$\mathbf{K}_x = \begin{bmatrix} -0.090 & 0.094 & 0.0 & 0.0 & 0.0 & -0.001 & 0.0 & 0.0 \\ 0.0 & 0.0 & -0.090 & 0.094 & 0.0 & 0.0 & 0.0 & -0.001 \\ 0.0 & -0.001 & 0.0 & 0.0 & -0.090 & 0.094 & 0.0 & 0.0 \\ 0.0 & 0.0 & 0.0 & -0.001 & 0.0 & 0.0 & -0.090 & 0.094 \end{bmatrix}.$$

The controller design is carried out for the nominal system without cross-coupling effects. A root locus with the non-conservative stiffness coefficient k_n as parameter shows the stability margin, which can be seen in Fig. 4.12. k_n starts at zero with all system poles located at $z_i = 0.97$. If k_n is larger than $9.4 \cdot 10^6$ N/m, the system becomes unstable unless the controller is adapted to the new parameters.

4.3.3 Predictor

After the state space model is assigned, the predictor used for the state space adaptive control has to be calculated. Additionally, this predictor is necessary to compute the estimated system states for the state space controller following the law

$$\begin{aligned} \hat{\mathbf{x}}(k+1,\mathbf{p}) &= \mathbf{A}(\mathbf{p})\,\hat{\mathbf{x}}(k,\mathbf{p}) + \mathbf{B}\,\mathbf{u}(k) + \mathbf{K}(\mathbf{p})\,\boldsymbol{\varepsilon}(k), \\ \hat{\mathbf{y}}(k) &= \mathbf{C}(\mathbf{p})\,\hat{\mathbf{x}}(k,\mathbf{p}), \\ \boldsymbol{\varepsilon}(k,\mathbf{p}) &= \mathbf{y}(k) - \hat{\mathbf{y}}(k|\mathbf{p}). \end{aligned}$$

Inputs to the predictor are the rotor positions $\mathbf{y}(k)$ determined by equation Eqn.(2.80) and Eqn.(2.79). Outputs are the estimated system states $\hat{\mathbf{x}}(k)$ which are inputs to the state space controller.

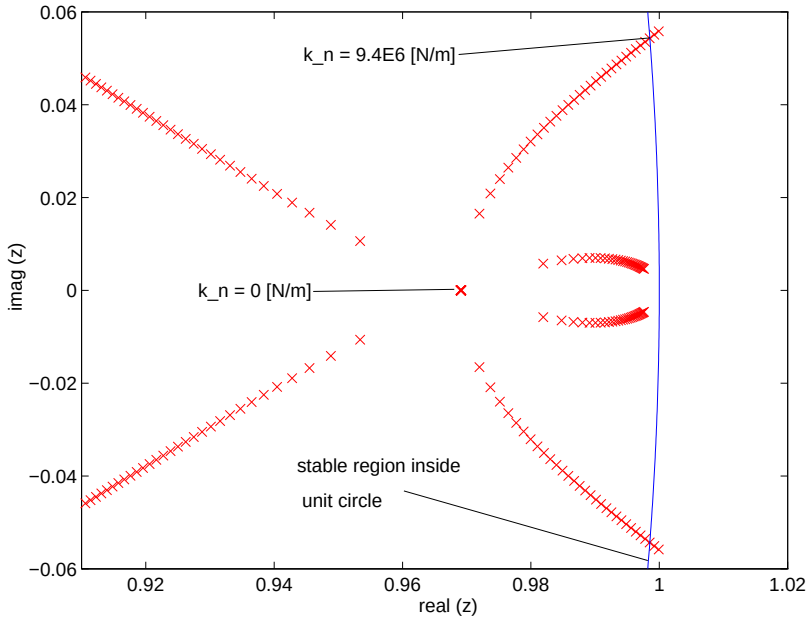

Figure 4.12: Root locus of the closed loop system with varying non-conservative stiffness parameter k_n from $0\,\mathrm{N/m}$ to $10^7\,\mathrm{N/m}$ and constant controller parameters. The closed loop system starting at $z_i = 0.97$ is unstable for $k_n > 9.4 \cdot 10^6\,\mathrm{N/m}$.

Since the system to be controlled is open loop unstable and the statistical properties of the system and measurement noise are not known in advance, the Kalman matrix has to be designed in advance, too. This deterministic approach can be done using pole placement for the state space model.

Similarly to the state space model in controller canonical form, a model can be derived in observer canonical form [Tolle, 1985]. If this model is used, the observer design can be carried out using the same procedure as for the controller design with all matrices transposed. The only design parameters are the poles of the initial predictor. Choosing these poles to be $z_i = 0.90$, which corresponds to a predictor being four times faster than the closed loop system, the resulting initial Kalman matrix becomes

$$\mathbf{K} = \begin{bmatrix} 1.1332 & 0.0 & 0.3535 & 0.0 \\ 1.1993 & 0.0 & 0.3717 & 0.0 \\ 0.0 & 1.1332 & 0.0 & 0.3535 \\ 0.0 & 1.1993 & 0.0 & 0.3717 \\ 0.3535 & 0.0 & 1.1181 & 0.0 \\ 0.3717 & 0.0 & 1.1834 & 0.0 \\ 0.0 & 0.3535 & 0.0 & 1.1181 \\ 0.0 & 0.3717 & 0.0 & 1.1834 \end{bmatrix}.$$

4.4 Closed loop dynamics

Once the controller and the predictor have been designed, the closed loop dynamics can be simulated in order to verify the desired behaviour of the controlled rotor bearing system. Additionally, simulations should show whether the linearisation of the actuator is justified and the linear state space controller can cope with both set point changes and disturbances like additional loads.

4.4.1 Initial values for simulation

Before a simulation run can be started the initial values for the controller and for all system variables have to be defined and chosen properly in advance.

All current control loops start at the point of operation defined by the bias current $i_0 = 4\,\mathrm{A}$ with all state variables like the initial flux Φ_0 and the control voltage u_c initialised properly for each channel similarly to Section 4.1.3.

The steady state force acting on the rotor, like the rotor weight, is compensated by a steady state magnetic force using the current control loops as described previously. Since no external forces act on the rotor, the rotor can be assumed to stay in a centred position and behave according to the derived state space model. The initial state vector is set equal to zero for this position as $\mathbf{x}(t=0) = \mathbf{0}$. The same is true for the estimated state vector $\hat{\mathbf{x}}(k=0) = \mathbf{0}$ with $\mathbf{u}(k=0) = \mathbf{0}$ and $\boldsymbol{\varepsilon}(k=0) = \mathbf{0}$.

4.4.2 System response to set point change

The closed loop system poles where placed at $z_i = 0.97$ or $s_i = -288\,1/\mathrm{s}$ for the controller with and without integrative feedback. In the following, system responses to a set point change are simulated for a P-structured and a PI-structured controller.

P-structure

A set point change is applied to the controlled system with $100\,\mu\mathrm{m}$ in each direction in both bearing planes, i.e. $\mathbf{W} = [100, 100, 100, 100]^T\,\mu\mathrm{m}$ (see Fig. 3.3). The resulting time history for the rotor displacements and the control currents can be seen in Fig. 4.13 and Fig. 4.14.

As mentioned previously, a steady state control current is added to the control current with $\mathbf{i}_{c_w} = \boldsymbol{K}_i^{-1} \cdot \mathbf{F}_w$. The current gain K_i is computed for the point of operation defined by $i_0 = 4\,\mathrm{A}$. Since the point of operation is shifted due to the additional load, a mismatch between the assumed system and the true system is generated with respect to the estimated coefficients for the active magnetic bearing. This results in the deviation of the rotor from the centre. Additionally, the controller parameters calculated from the estimated current gain and position stiffness cause a position error in y-direction.

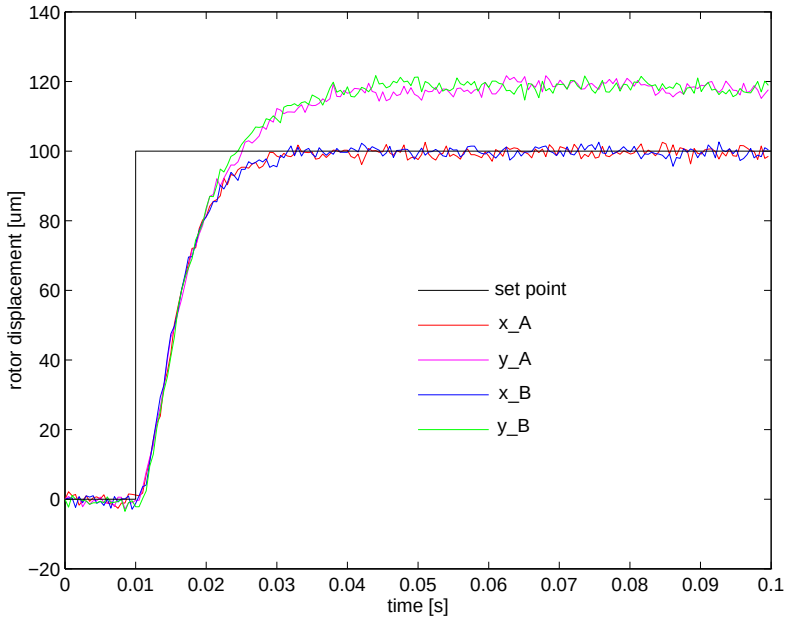

Figure 4.13: Time history of the rotor displacements after a set point change from zero to $\mathbf{W} = [100, 100, 100, 100]^T\,\mu$m *at time* $t = 0.01\,$s *(P-structured controller).*

PI-structure

A set point change is applied to the controlled system with $100\,\mu$m in each direction in both bearing planes, i.e. $\mathbf{W} = [100, 100, 100, 100]^T\,\mu$m (see Fig. 3.4). In this case an integrative feedback changes the steady state behaviour as shown in Fig. 4.15 for the time history of the rotor displacements and in Fig. 4.16 for the time history of the control currents, respectively. Note that no set point error remains if integrative feedback is added to the controller.

4.4.3 System response to additional load

In order to investigate the closed loop system behaviour with respect to external disturbances, an additional load is applied to the rotor, in this case 100 N in x-direction on both bearing A and bearing B.

P-structure

The additional load appears at $t = 0.01\,$s with 100 N for each bearing in x-direction. The time history of the rotor displacements and the control currents can be seen in Fig. 4.17 and Fig. 4.18, respectively.

The load of 100 N in x-direction causes a mean displacement of approximately $165\,\mu$m.

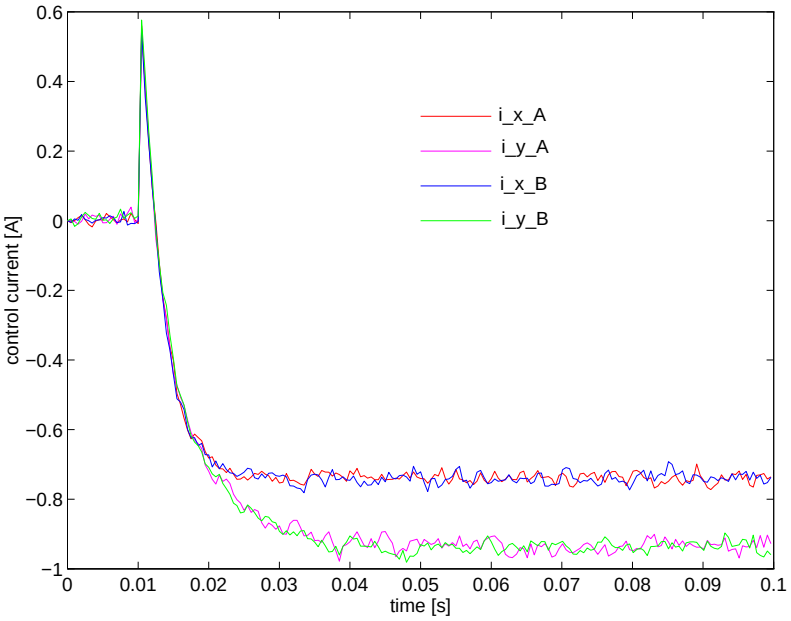

Figure 4.14: Time history of the control currents after a set point change from zero to $\mathbf{W} = [100, 100, 100, 100]^T\,\mu\text{m}$ *at time* $t = 0.01\,\text{s}$ *(P-structured controller).*

This yields a closed loop stiffness for the active magnetic bearing under state space control of $6 \cdot 10^6\,\text{N/m}$ or a flexibility of $1.65 \cdot 10^{-6}\,\text{m/N}$.

Note that in y-direction there is a slight deviation from the centre position, although the rotor weight is compensated by a steady state current. The reason for the deviation is the difference between the calculated stiffness factors for the point of operation and the real stiffness coefficients which depend on the new point of operation determined by the steady state currents. This effect appears independently from the additional load and can only be compensated by an iterative solution for the current gain of the magnetic actuator which depends on the steady state load, e.g. rotor weight. This load influences the steady state currents which are computed from the current gain.

PI-structure

A load of 100 N for each bearing is applied to the rotor at $t = 0.01\,\text{s}$ in x-direction. The corresponding time history of the rotor displacements and the control currents can be seen in Fig. 4.19 and Fig. 4.20, respectively.

As shown in Fig. 4.19 the advantage of an additional integrative feedback becomes obvious. Despite the additional load no deviation from the centred rotor position remains. This behaviour can be interpreted as an infinite gain of the actuator at a zero frequency and distinguishes a rotor bearing system using active magnetic bearings form ordinary rotor bearing systems.

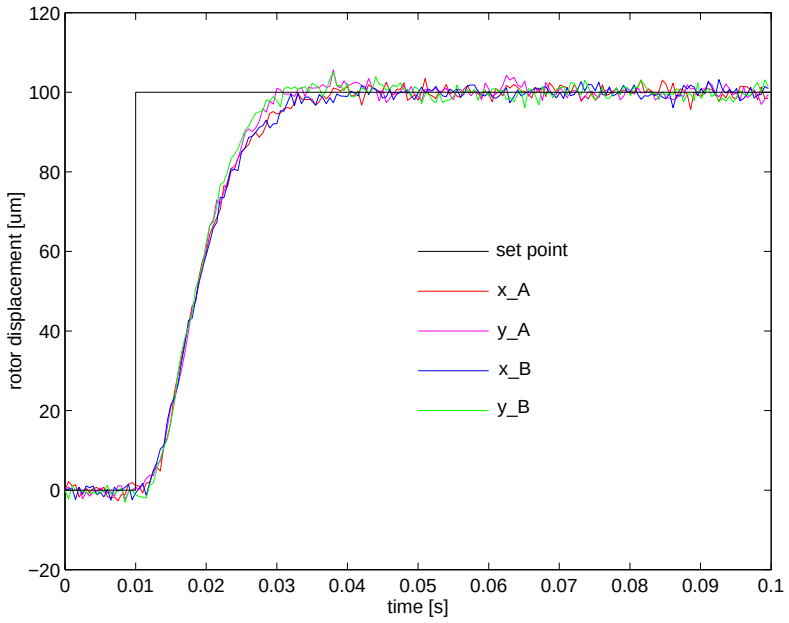

Figure 4.15: Time history of the rotor displacements after a set point change from zero to $\mathbf{W} = [100, 100, 100, 100]^T\,\mu\text{m}$ *at time* $t = 0.01\,\text{s}$ *(PI-structured controller).*

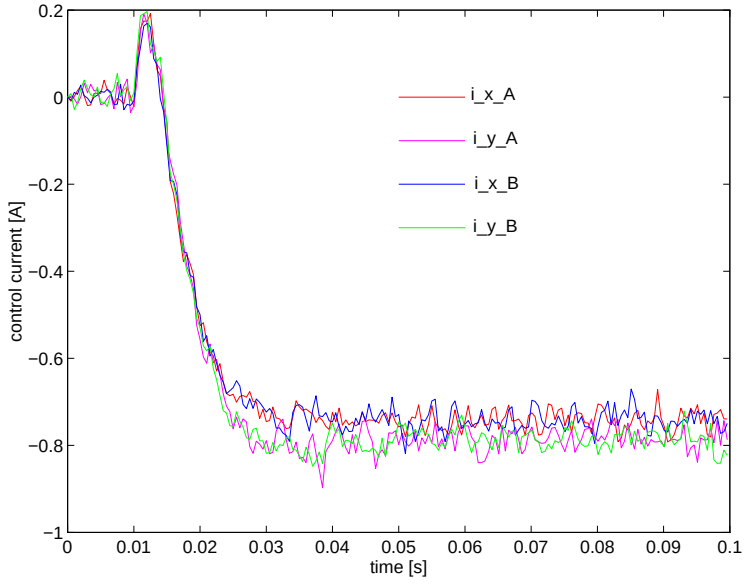

Figure 4.16: Time history of the control currents after a set point change from zero to $\mathbf{W} = [100, 100, 100, 100]^T\,\mu\text{m}$ *at time* $t = 0.01\,\text{s}$ *(PI-structured controller).*

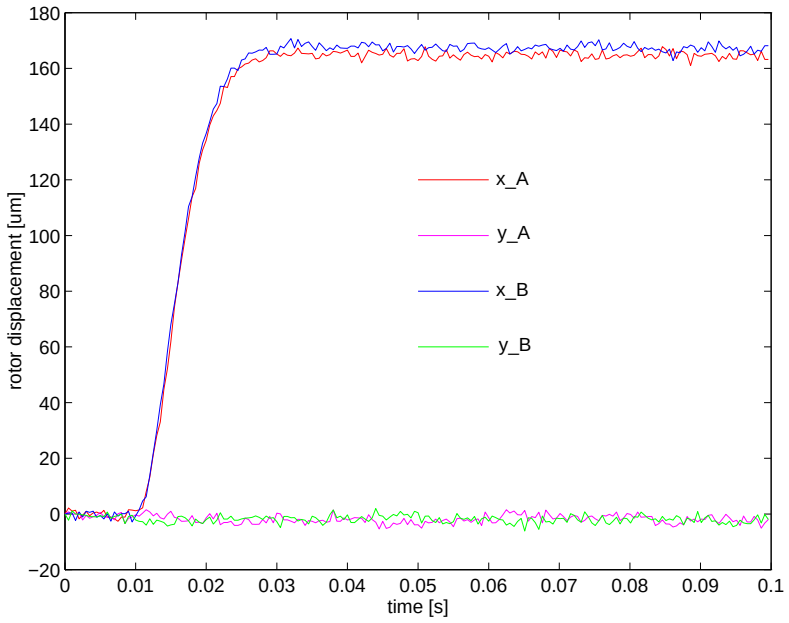

Figure 4.17: Time history of the rotor displacements after an additional load of $100\,\mathrm{N}$ *exerted to each bearing at time* $t = 0.01\,\mathrm{s}$ *(P-structured controller).*

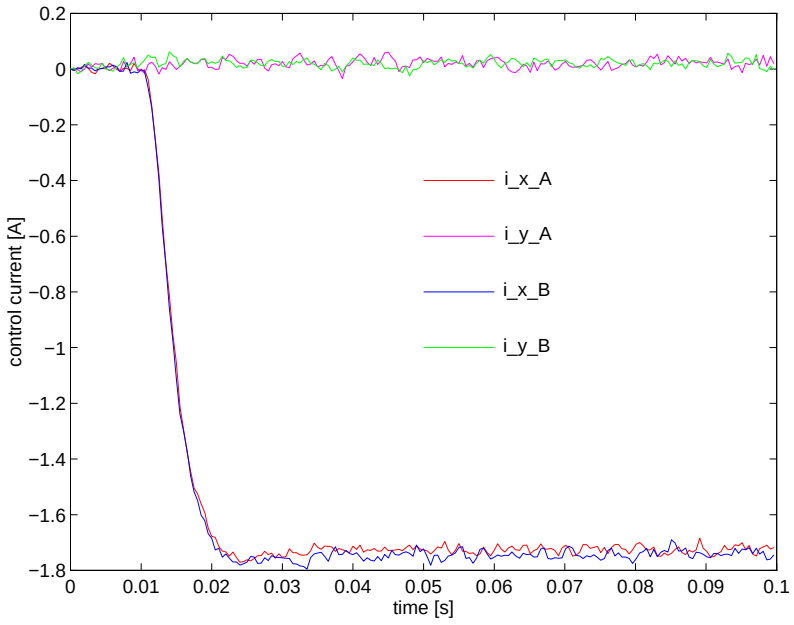

Figure 4.18: Time history of the control currents after an additional load of $100\,\mathrm{N}$ *exerted to each bearing at time* $t = 0.01\,\mathrm{s}$ *(P-structured controller).*

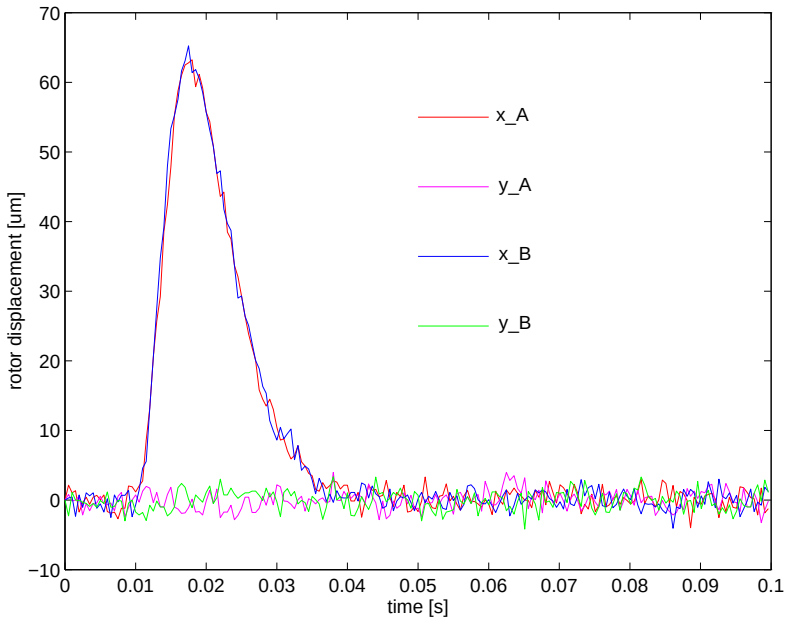

Figure 4.19: Time history of the rotor displacements after an additional load of $100\,\mathrm{N}$ *exerted to each bearing at time* $t = 0.01\,\mathrm{s}$ *(PI-structured controller).*

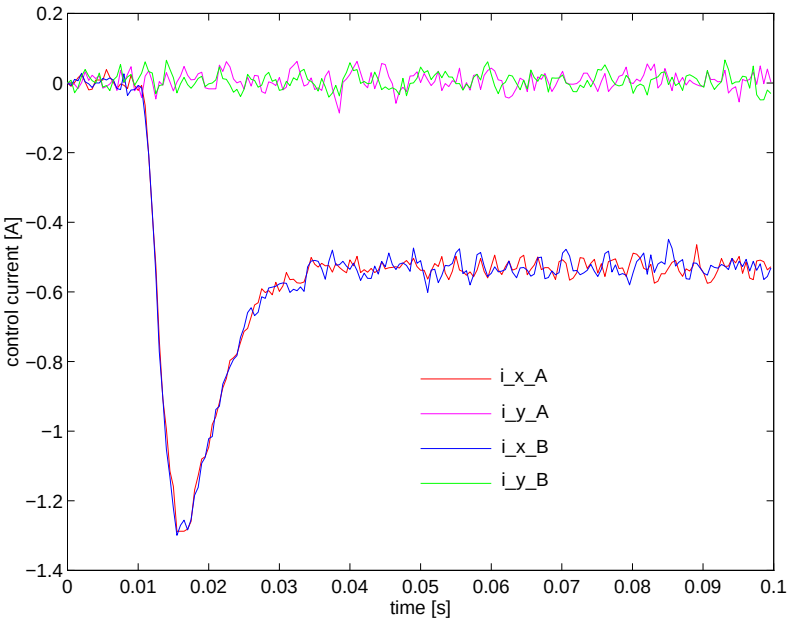

Figure 4.20: Time history of the control currents after an additional load of $100\,\mathrm{N}$ *exerted to each bearing at time* $t = 0.01\,\mathrm{s}$. *(PI-structured controller).*

4.5 State space adaptive control

The major objective of the presented work is the state space adaptive control for a rigid rotor suspended in two active magnetic bearings. After it has been shown that a state space controller based on a linear discrete time model of the plant is able to control the system, the adaptive control algorithm developed in Chapter 3 is implemented using a nonlinear plant model as described in detail in Chapter 2 with the block diagrams shown in Appendix D.1.

In order to simulate a change in system parameters, the sudden appearance of non-conservative cross-coupling forces as generated by seals of rotating machinery rotors is assumed. These forces change the system matrix by changing the skew-symmetric cross-coupling terms of the stiffness matrix in a given rotor plane. The step is considered to be the worst case in turbomachinery application, e.g. a sudden pressure loss or leakage in sealings leads to a parameter change in a linear model. Actually, the effect of the cross-coupling forces develops slowly, and an abrupt change in the non-conservative stiffness parameter can be considered as a worst case scenario.

In the following all initial values necessary for both simulation and for a real time implementation are considered.

4.5.1 Initial values for simulation

Before a simulation run can be started the initial values for the adaptive control and for all system variables have to be defined and chosen properly in advance.

Initial system states

For the simulation of a parameter change all initial state values are set equal to the initial values for a set point change as described in the previous section, namely $\mathbf{x}(t = 0) = \mathbf{0}$, $\hat{\mathbf{x}}(k = 0) = \mathbf{0}$, $\mathbf{u}(k = 0) = \mathbf{0}$, and $\boldsymbol{\varepsilon}(k = 0) = \mathbf{0}$.

Initial parameters and covariance matrix

In contrast to most applications of adaptive control, the initial parameters in the parameter vector $\mathbf{p}$ are assumed to be the true ones with a rather small covariance $\mathbf{P}$. Usually, the initial parameters are chosen equal to zero with a high covariance. If the plant to be identified is open loop stable and the identification is performed in an open loop mode, this approach suits very well and the parameters to be estimated converge fast. Since an unstable plant has to be identified in closed loop, the choice of the initial parameters is more complex.

A parameter error may cause instability from the beginning, because the controller parameters depend on the initial parameters. If these are false, the control action is wrong as well. Therefore, the initial parameters for the estimation algorithm are set

equal to the *a priori* values, derived from the linear state space model in controller canonical form.

A large covariance has similar effects on wrong system parameters, since the parameters change very quickly. Therefore, the initial covariance is set to a rather small value of $\mathbf{P} = 10^{-8} \cdot \mathbf{I}$. The covariance is only increased if a parameter change is triggered by using the forgetting factor.

Initial forgetting factor

The forgetting factor $\rho(k)$ determines the change of the covariance matrix, i.e. its increase or decrease. The initial value is chosen to be $\rho(k = 0) = 1$ which corresponds to practically no forgetting, or heuristically speaking, the initial parameters are believed to be the true ones.

4.5.2 Implementation of the state space adaptive controller

The control algorithm is coded with the numerical engineering tool MATLAB with its functions given in Appendix D.2 [MATLAB, 1992]. The algorithm includes the parameter estimation algorithm, the computation of the controller parameters based upon the estimated system parameters, the predictor, and the state space controller. All functions are executed at each sampling period by the simulation program.

Since the state space adaptive controller is implemented separately from the simulation model, the porting to a real application should be easier. The nonlinear model itself is executed at a integration frequency of 1 MHz using the Runge-Kutta algorithm [SIMULINK, 1992]. This yields a simulation step size of 1 μs, which is very small, but necessary in order to render the behaviour of the switching amplifiers. Otherwise the zero crossings are not hit exactly which results in additional parasitic noise.

4.5.3 System response due to parameter change

After the initial values have been set, the rotor, suspended on two active magnetic bearings, is simulated in the MATLAB/SIMULINK environment. Although the rotor runs at a speed of $20,000$ rpm, no unbalance forces are considered, because the unbalance response conceal instability. This is done only to show whether the control concept works or not. The so controlled rotor bearing system is then exposed to a parameter change in order to test the adaptive control concept. Simulation runs have been carried out for both a simple state space controller and a state space controller with additional integrative feedback.

P-structure

The closed loop system controlled by a simple state space controller is investigated with respect to a parameter change at $t = 0.01$ s applied to the system by a sudden

appearance of cross-coupling forces with a skew-symmetric non-conservative stiffness factor of $k_n = 6 \cdot 10^6$ N/m at a given plane along the rotor axis determined by the parameter n given in Tab. 2.4.

Immediately after the parameter change the system is unstable in terms of its structure, but the displacements increase slowly. When a certain signal to noise ratio is achieved, the parameter change is recognised by the algorithm. In other words, if the variance of the prediction error increases and thus the forgetting control factor $\delta(k)$ presented in Eqn.(3.48) passes a certain threshold, the parameters are assumed to have changed. Therefore, the forgetting factor is set to a smaller value, in this case $\rho_0 = 0.999$. The corresponding plots can be seen in Fig. 4.21.

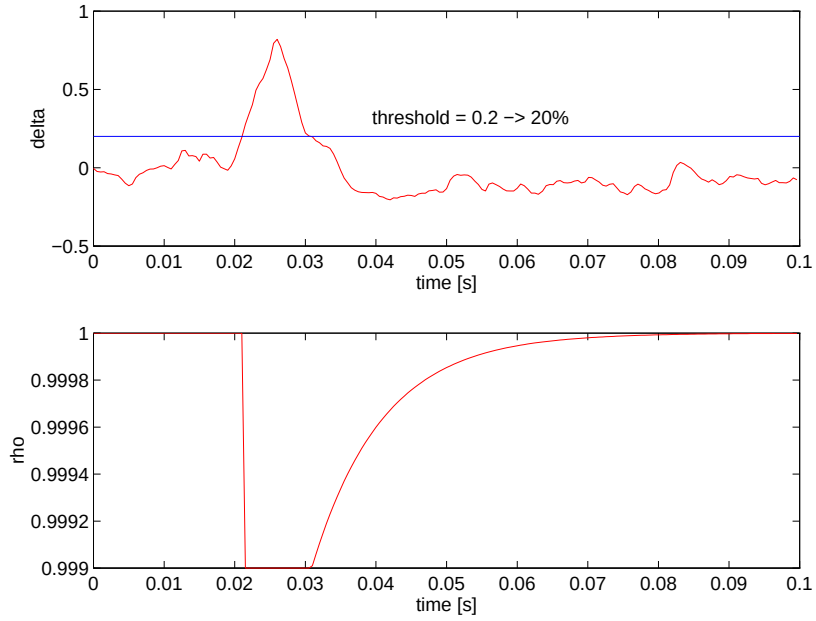

Figure 4.21: Time history of the forgetting control variable δ and the forgetting factor ρ, after the appearance of a non-conservative cross-coupling stiffness of $k_n = 6 \cdot 10^6$ N/m at time $t = 0.01$ s (P-structured controller).

In addition to the reset of $\rho(k)$, a white noise signal with the arbitrarily chosen maximum deflection of 100 μm is added to the set point. This generates a ripple on the control variable, because the set point is fed through the feed forward matrix $\mathbf{K}_w$, and excites the entire system. Since this part of the control variable is not correlated to the estimation error generated by the measurement noise, the signal to noise ration increases which makes the algorithm converge faster. A plot of the set point can be seen in Fig. 4.22. The burst signal is added to the set point as long as $\rho(k)$ remains reset, i.e. as long as $\delta(k)$ is larger than the threshold.

Parallel to the identification, the controller parameters are calculated according to Eqn.(3.70) and Eqn.(3.71). It can be observed that the feedback gain matrix of the

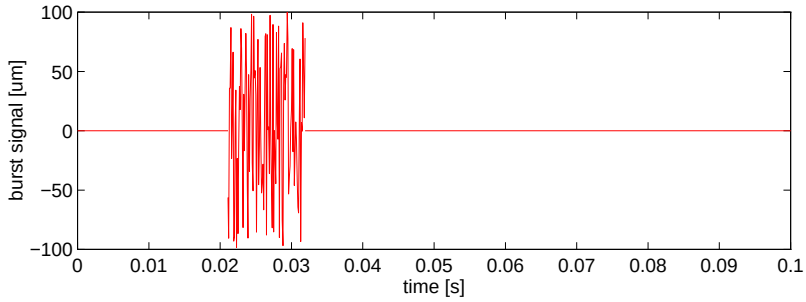

Figure 4.22: Time history of the white noise burst signal added to the set point, when a parameter change is triggered (P-structured controller).

state space controller becomes non-symmetric to the same extent as the parameter of the non-conservative stiffness does. This effect can easily be seen in Eqn.(3.70). These non-symmetric entries in the controller matrix cause a force, which directly compensates the non-conservative forces of the system. Due to the adaptation of the controller the rotor bearing system can recover from a destabilising parameter change.

The time history of the rotor displacements and the control currents can be seen in Fig. 4.23 and Fig. 4.24, respectively.

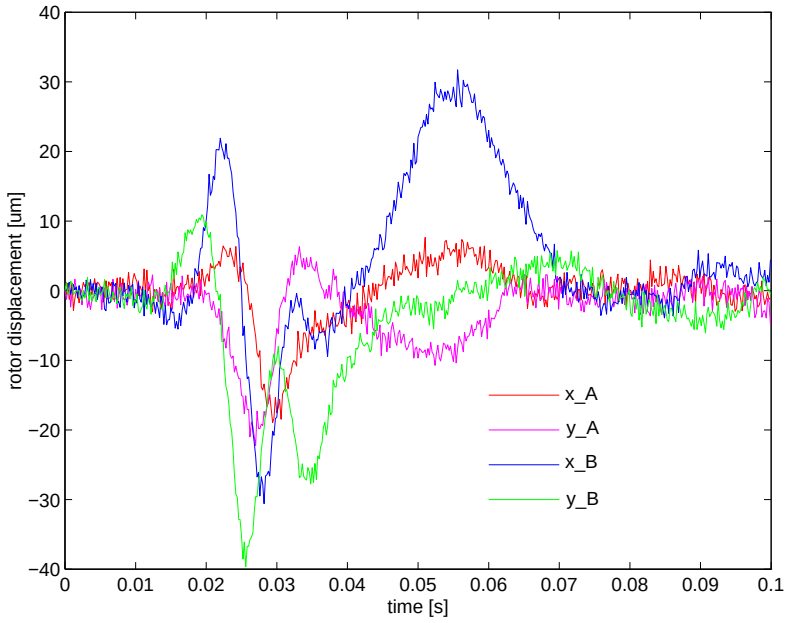

Figure 4.23: Time history of the rotor displacements after the appearance of a non-conservative cross-coupling stiffness of $k_n = 6 \cdot 10^6\,\mathrm{N/m}$ *at time* $t = 0.01\,\mathrm{s}$ *(P-structured controller).*

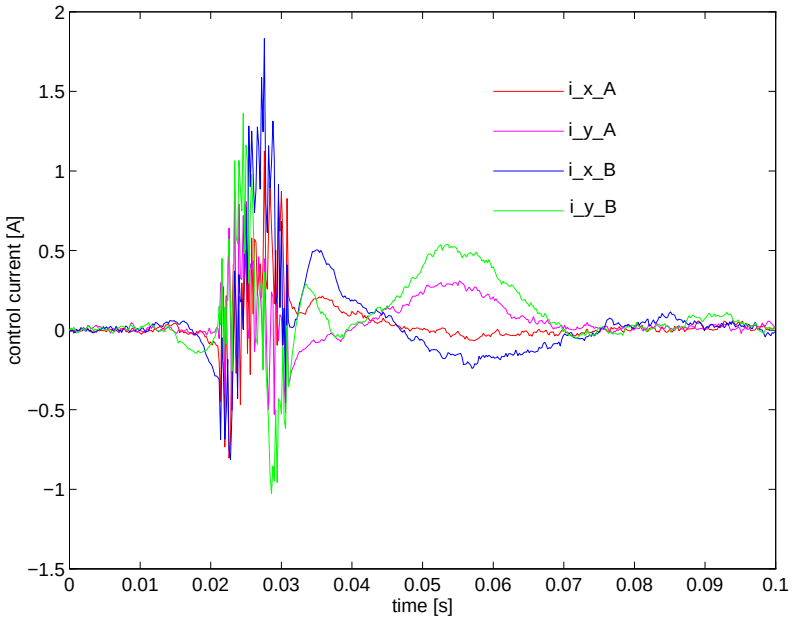

Figure 4.24: Time history of the control currents after the appearance of a non-conservative cross-coupling stiffness of $k_n = 6 \cdot 10^6\,\mathrm{N/m}$ *at time* $t = 0.01\,\mathrm{s}$ *(P-structured controller).*

In total $n_p = 96$ parameters are adapted, but only few of them change significantly. This is due to the fact that not every parameter is affected by the change of the non-conservative stiffness factor to the same extent. Note that the parameters in the parameter vector $\mathbf{p}$ depend on discrete time state space matrices, and have neither a specific unit nor a unique physical meaning.

Investigations with parameter variations have shown, whether a physical parameter influences a parameter in the discrete time state space model. It turned out that one physical parameter can influence more discrete model parameters and vice versa. But the trace of certain parameters as for example rotor mass or the skew-symmetric non-conservative stiffness parameter could be followed. The rotor mass mainly affects the sub-matrices in the diagonal of the system matrix $\mathbf{A}$, i.e. the parameters a_m^{ii} with $m = 1, 2$ and $i = 1, 2, 3, 4$. The non-conservative stiffness parameter influences some non-symmetric entries of the the system matrix $\mathbf{A}$.

The parameter $\mathbf{p}(1)$, is equal to $-a_2^{11}$ of the system matrix $\mathbf{A}$ and depends mainly on the rotor mass. Therefore, it is obvious that this parameter does not change significantly. The time history of this parameter can be seen in Fig. 4.26 in Fig. 4.25.

A second parameter, $\mathbf{p}(8)$ is equal to to $-a_1^{14}$, a non-symmetric entry of the system matrix $\mathbf{A}$ which is of course affected by the skew-symmetric non-conservative stiffness parameter. The time history of this parameter can be seen in Fig. 4.26.

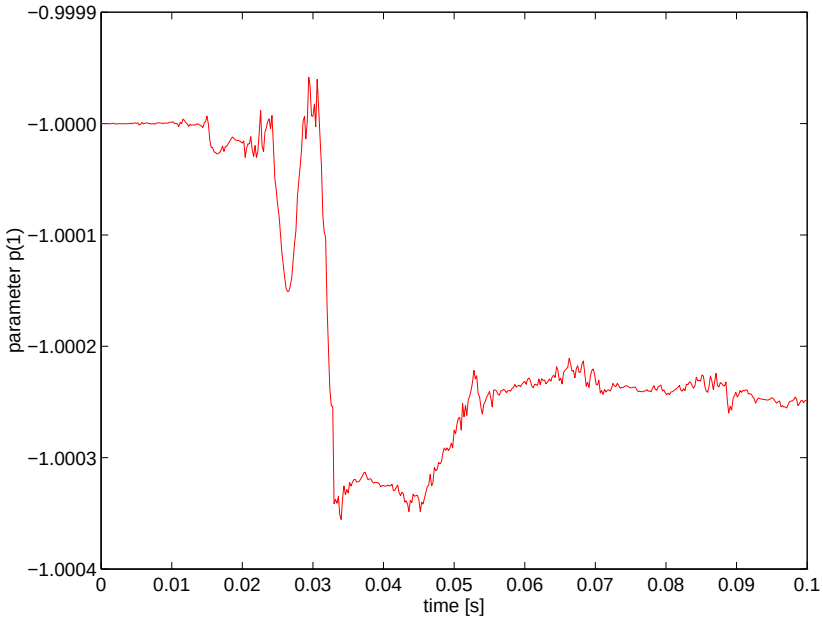

Figure 4.25: Time history of a sample system parameter $\mathbf{p}(1)$ *after the appearance of a non-conservative cross-coupling stiffness of* $k_n = 6 \cdot 10^6\,\mathrm{N/m}$ *at time* $t = 0.01\,\mathrm{s}$ *(P-structured controller).*

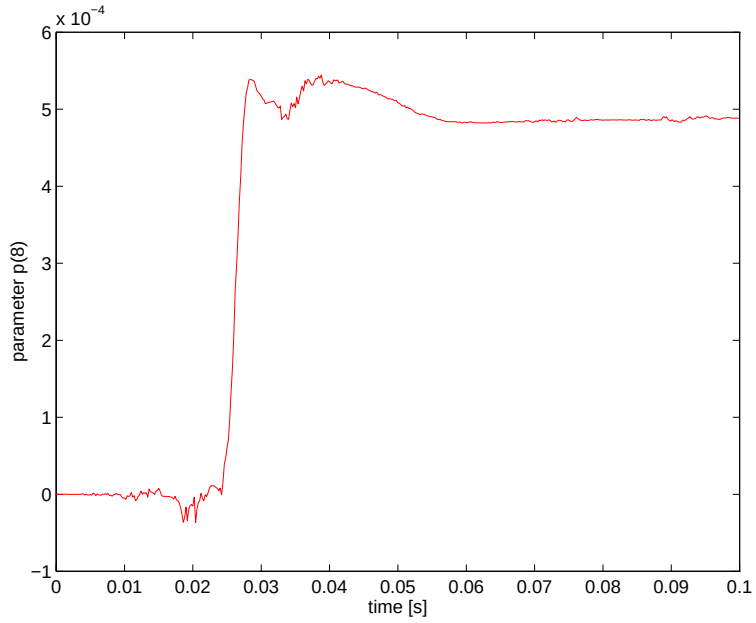

Figure 4.26: Time history of a sample system parameter $\mathbf{p}(8)$ *after the appearance of a non-conservative cross-coupling stiffness of* $k_n = 6 \cdot 10^6\,\mathrm{N/m}$ *at time* $t = 0.01\,\mathrm{s}$ *(P-structured controller).*

PI-structure

In this case, the closed loop system is controlled by a state space controller with additional integrative feedback. A parameter change at $t = 0.01\,\mathrm{s}$ is then applied to the system by a sudden appearance of cross-coupling forces with a non-conservative stiffness factor of $k_n = 6 \cdot 10^6\,\mathrm{N/m}$.

The behaviour of the entire system under adaptive control is very similar to a system controlled by a simple state feedback controller. The parameter change is triggered a little later, because the stability region is larger for a system with integrative feedback as shown in Fig. 4.12. The history of the forgetting control factor and the plot of the forgetting parameter can be seen in Fig. 4.27. Additionally, a white noise signal

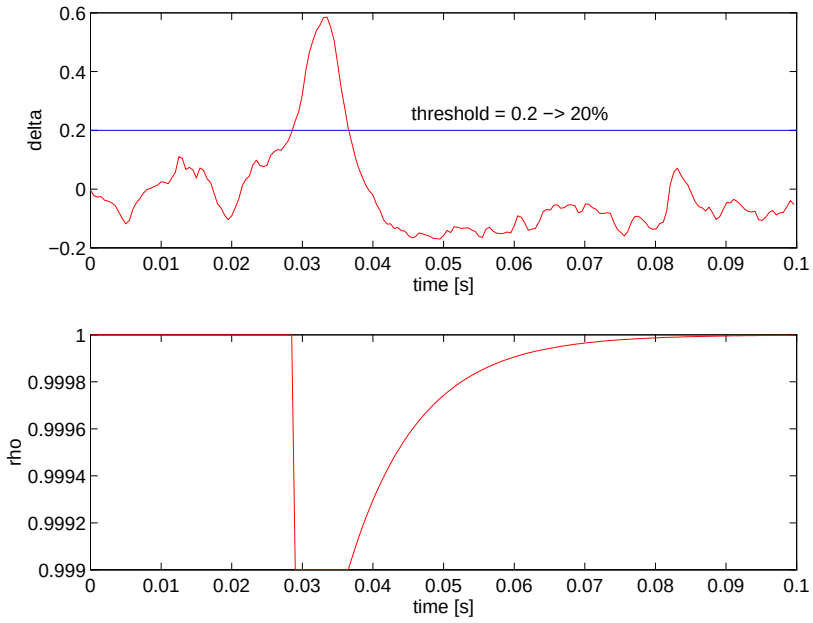

Figure 4.27: Time history of the forgetting control variable δ and the forgetting factor ρ. after the appearance of a non-conservative cross-coupling stiffness of $k_n = 6 \cdot 10^6\,\mathrm{N/m}$ at time $t = 0.01\,\mathrm{s}$ (PI-structured controller).

with a maximum deflection of $100\,\mu\mathrm{m}$ is added to the set point. This generates only a small ripple on the control variable, because the set point is not directly fed through the feed forward matrix $\mathbf{K}_w$, but passes the integrative loop, which is a low pass. Nevertheless, a control variable is generated which is not correlated to the estimation error generated by the measurement noise. The adaptation is performed similarly to the case with a simple state feedback controller and the rotor bearing system recovers from the parameter change. The time history of the rotor displacements and the control currents can be seen in Fig. 4.28 and Fig. 4.29, respectively. The time history of the strongly changing parameter $\mathbf{p}(8)$ can be seen in Fig. 4.30, the time history of the parameter $\mathbf{p}(1)$ with very little change can be seen in Fig. 4.31.

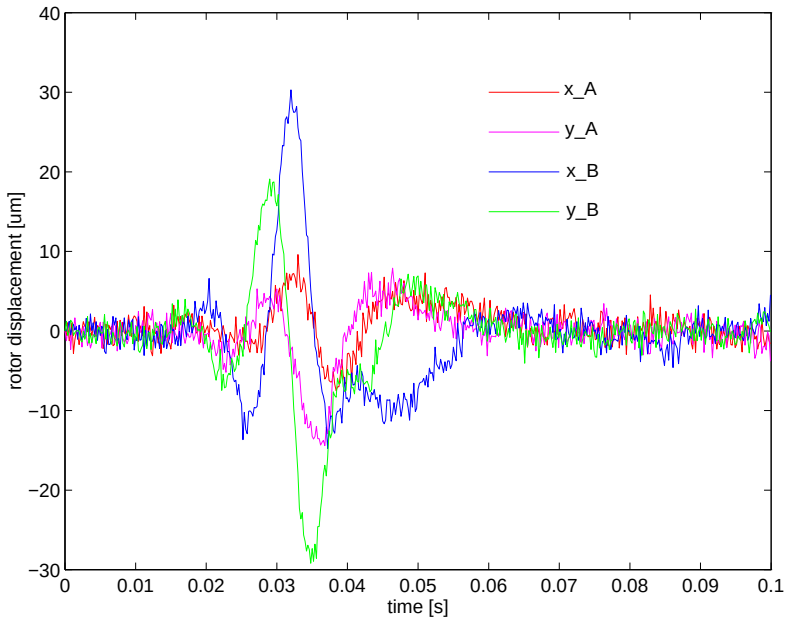

Figure 4.28: Time history of the rotor displacements after the appearance of a non-conservative cross-coupling stiffness of $k_n = 6 \cdot 10^6\,\mathrm{N/m}$ *at time* $t = 0.01\,\mathrm{s}$ *(PI-structured controller).*

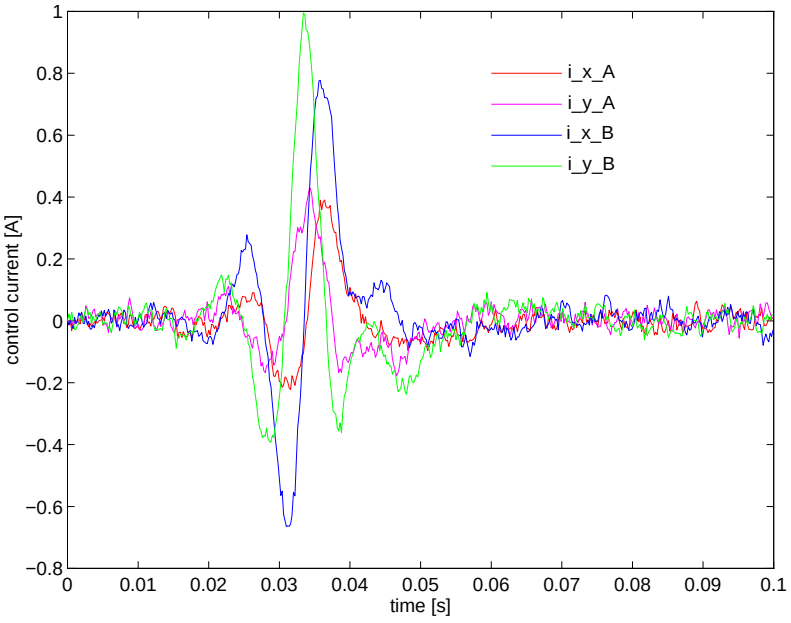

Figure 4.29: Time history of the control currents after the appearance of a non-conservative cross-coupling stiffness of $k_n = 6 \cdot 10^6\,\mathrm{N/m}$ *at time* $t = 0.01\,\mathrm{s}$ *(PI-structured controller).*

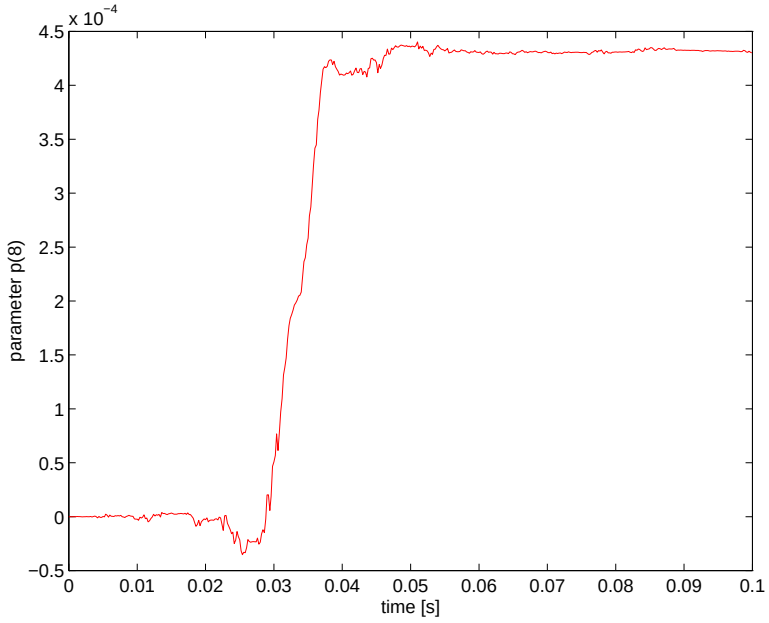

Figure 4.30: Time history of a sample system parameters $\mathbf{p}(8)$ *after the appearance of a non-conservative cross-coupling stiffness of* $k_n = 6 \cdot 10^6\,\mathrm{N/m}$ *at time* $t = 0.01\,\mathrm{s}$ *(PI-structured controller).*

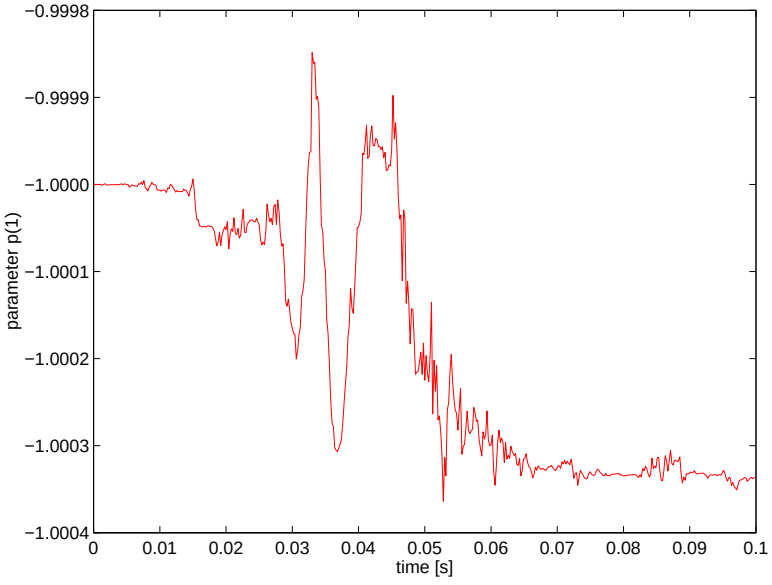

Figure 4.31: Time history of a sample system parameter $\mathbf{p}(1)$ *after the appearance of a non-conservative cross-coupling stiffness of* $k_n = 6 \cdot 10^6\,\mathrm{N/m}$ *at time* $t = 0.01\,\mathrm{s}$ *(PI-structured controller).*

4.5.4 Discussion of the numerical results

The problem involved with state space adaptive control for a rotor suspended in active magnetic bearings is the fast dynamic behaviour of the open loop plant, which is unstable in addition. Usually, control is applied to compensate disturbances or make the closed loop faster than the open loop system. For the rotor bearing system presented in this work, the closed loop eigenvalues have the same absolute values as the open loop ones. If the open loop system is slower than the closed loop system, there is more time to adapt the system. If the open loop system has a fast and unstable behaviour, the time for parameter adaptation is limited. In a pure linear case, this time restriction would infer no problems. If the system is bounded by saturation, however, the dynamical range underlies certain constraints. These are mainly the constraints for displacement and the control current. Although the adaptive control concept is limited in the range of parameter changes, two regions of positive operation remain.

Parameter change does not destabilise the closed loop system

If a parameter change does not destabilise the system, all closed loop system poles lie inside the unit circle. In this first case, the adaptation process lasts very long, which is not a problem as long as the system is stable. This is due to the fact that the output signal contains only little information on the process, because the entire system is only excited by the measurement noise corrupting the output. Moreover, the control variable is correlated with the output variable. An uncorrelated part of the control variable is needed in order to estimate the parameters of the system under investigation quickly and adapt to parameter changes. This requirement could be satisfied by set point changes. Since the main objective of the control for a rotor bearing system is the stabilisation and compensation of disturbances, set point changes are undesirable. Another possibility to excite the system would be by a white noise signal added to the zero set point with a larger amplitude than the measurement noise. This procedure, however, is not applicable, because unnecessary vibrations are generated.

Parameter change destabilises the closed loop system

The second case is that a parameter change destabilises the system. Here, the closed loop poles are moved outside the unit-circle in the z-plane, or into the right half complex plane in the continuous time domain. The new poles determine the speed of the destabilisation process, i.e. the time delay until the rotor touches the backup bearing or the amplifiers reaches saturation. This means that the adaptation algorithm has to adapt the system parameters and hence the controller parameters within a certain time and without making the controller run into saturation. Roughly speaking, the adaptation law has to move the closed loop poles back into the stability region, i.e. inside the unit circle.

The speed of the adaptation algorithm is determined by the value of the forgetting factor and the covariance of the parameters to be estimated. Of course, a large covariance covers many parameter changes for systems with slow dynamics. As for the

presented system, a large covariance destabilises the system, because unstable predictors are generated permanently, which violate the stability criterion for the adaptation procedure. Therefore, the covariance has to be kept rather small, which could be proved by means of simulation as well. Otherwise the entire system becomes unstable even if there is no parameter change.

The forgetting factor is the second parameter determining the adaptation speed in two ways. On the one hand, a low forgetting factor means that the parameters are considered to be false and the newly estimated are "more true". Then the parameters can change quickly and adapt to the new situation, but generate unstable predictors as well, which destabilise the adaptive control loop in the end. On the other hand the covariance is increased fast if the forgetting factor is too low. This leads to the aforementioned problem of unstable predictors. What remains is a dilemma. Either the system is destabilised by parameter changes with the adaptation algorithm being too slow due to a small covariance, or by unstable predictors with the covariance being too large.

Whether the adaptation algorithm can follow a parameter change finally depends on the covariance and the forgetting factor within certain constraints:

- If the initial covariance is too large from the beginning ($\mathbf{P} > 10^{-6} \cdot \mathbf{I}$), unstable predictors result.
- If the covariance is small enough ($\mathbf{P} < 10^{-6} \cdot \mathbf{I}$), and if
  - the forgetting factor is too small ($\rho(k) \ll 0.999$) a large variance of the system parameters is caused which finally destabilises the system.
  - the forgetting factor is chosen properly ($\rho(k) \approx 0.999$), the adaptation algorithm can cope with the parameter change.
  - the forgetting factor is too large ($\rho(k) \approx 1$), the system runs into saturation before the algorithm adapts to the true parameters.

As a conclusion it can be pointed out that the algorithm for adaptive control presented in this work performs excellently for a certain range of parameter changes. If these are too large instability cannot be prevented.